Clay Minerals (2023), **57**, 230–240
doi:10.1180/clm.2022.41

CAMBRIDGE UNIVERSITY PRESS

Article

Adsorption of lead by kaolinite, montmorillonite, goethite and ferrihydrite: performance and mechanisms based on quantitative analysis

Xiao Mao, Haibo Liu*, Ziyang Chu, Tianhu Chen, Xuehua Zou, Dong Chen, Xuemei Zhang and Jinchao Hu
Key Laboratory of Nano-Minerals and Pollution Control of Anhui Higher Education Institutes, Hefei University of Technology, Hefei 230009, China

Abstract

This work elucidated the performance and mechanisms of Pb^{2+} adsorption by kaolinite, montmorillonite, goethite and ferrihydrite using batch experiments. The contributions of various adsorption mechanisms were quantified using a stepwise extraction method. Several characterizations (scanning electron microscopy, X-ray diffraction, Fourier-transform infrared spectroscopy, point of zero charge analysis and X-ray fluorescence) were utilized to analyse the physicochemical properties and the potential adsorption mechanisms. The results indicated that the adsorption processes of montmorillonite and goethite approached equilibrium within 20 min, while 60 min were required for the adsorption processes of kaolinite and ferrihydrite. The adsorption processes of Pb^{2+} by the four minerals best fit the pseudo-second order model. The adsorption capacities of the four minerals for Pb^{2+} followed the order: montmorillonite > goethite > ferrihydrite > kaolinite, and the maximum adsorption capacities were 69.20, 46.95, 34.32 and 18.62 mg g^{-1}, respectively. The stepwise extraction test showed that the adsorption mechanism of Pb^{2+} was dominated by ion exchange for montmorillonite, precipitation and complexation for goethite and complexation for kaolinite and ferrihydrite.

Keywords: adsorption mechanism, lead, quantitative, soil minerals

(Received 25 August 2022; revised 5 December 2022; Accepted Manuscript online: 9 December 2022; Associate Editor: Balwant Singh)

Clay minerals and iron oxide minerals are common solid-phase components in soils. Clay minerals (including kaolinite, montmorillonite, illite, sepiolite, *etc.*) are composed mainly of hydrated magnesium–aluminium silicates (Uddin, 2017; Guo *et al.*, 2020; Zhou *et al.*, 2022). Iron oxides found in soils include goethite, ferrihydrite and hematite, among others (Ma *et al.*, 2019; Lai *et al.*, 2021). Soil minerals constitute an important medium for the accumulation of heavy-metal ions on account of their large specific surface area and abundant surface-adsorption sites, leading to favourable adsorption capacities for lead (Pb^{2+}), cadmium (Cd^{2+}), zinc (Zn^{2+}) and other metal ions (Bedelean *et al.*, 2009; Mbaye *et al.*, 2014; Vhahangwele & Mugera, 2015; Yin *et al.*, 2016; Lin *et al.*, 2019; Otunola & Ololade, 2020).

Lead, one of the common 'five toxic elements' in ecosystems, is non-biodegradable, accumulable and biotoxic (Bourliva *et al.*, 2013; Rui *et al.*, 2019; Ramola *et al.*, 2020). The adsorption characteristics and mechanisms of Pb^{2+} on various soil minerals vary significantly. Zhang & Hou (2008) demonstrated that the adsorption mechanism of Pb^{2+} on montmorillonite could be ascribed chiefly to the chemical binding of Pb^{2+} to surface hydroxyl groups and electrostatic binding. Tang *et al.* (2009) observed that the adsorption of Pb^{2+} on kaolinite occurred through ion exchange and complexation. Trivedi *et al.* (2003) proposed that Pb^{2+} was adsorbed on ferrihydrite mostly through inner-sphere complexation. The adsorption mechanism determines the occurrence state of Pb^{2+} in soils, which in turn affects the fate of Pb^{2+}. However, quantification of the adsorption mechanisms of Pb^{2+} by soil minerals (*e.g.* montmorillonite, goethite, ferrihydrite, kaolinite) has been determined only rarely. It has been reported that stepwise extraction could quantify the contributions of adsorption mechanisms, improving understanding of the occurrence state and stability of metal ions. For instance, Shen *et al.* (2017) quantified the contributions of exchangeable state (1.38–4.29%), precipitation (75.61–85.76%) and complexation (10.40–22.86%) adsorption mechanisms for Pb^{2+} adsorbance on three biochars. Cao *et al.* (2019) quantified the adsorption mechanism of Pb^{2+} on wheat straw biochar, in which the contributions of major adsorption mechanisms such as ion exchange and precipitation were 74.79% and 21.92%. These studies quantifying adsorption mechanisms through stepwise extraction have focused on biochars. However, current research on the mechanism of Pb^{2+} adsorption by montmorillonite, goethite, ferrihydrite and kaolinite has focused mostly on qualitative analysis, while quantitative analysis of this topic has been limited. Therefore, the quantification of the adsorption mechanisms of Pb^{2+} by montmorillonite, goethite, ferrihydrite and kaolinite based on stepwise extraction has important theoretical significance for our in-depth understanding of the occurrence state of Pb^{2+} in soils.

In the present work, the Pb^{2+} adsorption properties and mechanisms by montmorillonite, goethite, ferrihydrite and kaolinite were investigated using batch adsorption tests and

*Email: liuhaibosky116@hfut.edu.cn
Cite this article: Mao X, Liu H, Chu Z, Chen T, Zou X, Chen D, Zhang X, Hu J (2023). Adsorption of lead by kaolinite, montmorillonite, goethite and ferrihydrite: performance and mechanisms based on quantitative analysis. *Clay Minerals* **57**, 230–240. https://doi.org/10.1180/clm.2022.41

characterization techniques. The contributions of various adsorption mechanisms were quantified using a stepwise extraction method to provide the theoretical foundations for an in-depth understanding of the occurrence state of Pb^{2+} in soils.

Materials and methods

Chemicals and materials

Iron nitrate nonahydrate ($Fe(NO_3)_3{\cdot}9H_2O$) was kindly provided by the Zhiyuan Chemical Reagent Co., Ltd (Tianjin, China). Analytical reagents of lead nitrate ($Pb(NO_3)_2$), nitric acid (HNO_3), sodium hydroxide (NaOH) and potassium hydroxide (KOH) were manufactured by Sinopharm Chemical Reagent Co., Ltd (Shanghai, China).

The kaolinite was collected from Yangshan, Suzhou, China, and the X-ray fluorescence (XRF) results showed that the kaolinite was composed mainly of SiO_2 (49.41 wt.%), Al_2O_3 (46.35 wt.%), Fe_2O_3 (1.14 wt.%) and others (3.10 wt.%). The montmorillonite was collected from Chifeng City Wuhuatianbao Mineral Materials Co., Ltd (Inner Mongolia, China). According to our previous work, the montmorillonite was composed of SiO_2 (69.46 wt.%), Al_2O_3 (17.30 wt.%), Fe_2O_3 (6.77 wt.%), MgO (2.75 wt.%), CaO (1.97 wt.%) and others (1.75 wt.%) based on the XRF results (Zhang *et al.*, 2022). The preparation of goethite was done according to the process described by Notini *et al.* (2018) and synthesized *via* the hydrothermal method of mixing $Fe(NO_3)_3{\cdot}9H_2O$ and KOH in an alkaline environment. Ferrihydrite was prepared according to the method of Schwertmann & Cornell (2008), where $Fe(NO_3)_3{\cdot}9H_2O$ was dissolved and then the pH of the solution was adjusted to 7–8 with NaOH, allowing Fe^{3+} hydrolysis to generate ferrihydrite. All samples were ground and passed through a 0.075 mm sieve and then placed in a desiccator.

Characterization

The composition and crystal structure of the four minerals before and after Pb^{2+} adsorption were examined using X-ray diffraction (XRD; DX-2700, Dandong, China) at a scanning angle of 5–70°2θ. The morphologies and elemental distributions of the four minerals with and without Pb^{2+} adsorption were examined using scanning electron microscopy (SEM; Hitachi SU8020; Hitachi, Tokyo, Japan). The functional groups of the four minerals with and without adsorption of Pb^{2+} were recorded using a Fourier-transform infrared (FTIR) spectrometer (VERTEX 70; Bruker, Germany) in the wavelength range of 400–4000 cm^{-1}. The ζ-potential measurements of the four minerals were conducted at pH 1–12 using a Zetasizer Nano-ZS90 (Malvern Instruments, Inc., Malvern, UK). The isoelectric points of the four minerals were determined from their ζ-potentials and pH values (Fang *et al.*, 2014). The distribution of Pb^{2+} species in the pH range of 1–12 was simulated using *Visual MINTEQ* 3.1.

Batch adsorption experiments

The effects of initial concentration (5, 10, 20, 50, 80, 100 mg L^{-1}) and reaction time (5, 10, 20, 40, 60, 120, 180, 240 min) on the adsorption behaviour of Pb^{2+} by montmorillonite, goethite, ferrihydrite and kaolinite were studied using batch experiments. All Pb^{2+} solutions were obtained by diluting 10 g L^{-1} $Pb(NO_3)_2$. The 0.5 g L^{-1} adsorbent was added into a polypropylene centrifuge tube containing Pb^{2+} solutions at various pH values (4, 5 or 6). The mixture was shaken continuously for a certain period of time (ranging between 5 and 240 min). Then, the concentration of Pb^{2+} was measured using a flame atomic adsorption spectrophotometer (wys-2200, Wayeal, China).

Stepwise extraction of adsorbed Pb^{2+}

In this study, by following the approaches of Shen *et al.* (2017) and Tessier *et al.* (1979), the adsorption capacities of montmorillonite, goethite, ferrihydrite and kaolinite for Pb^{2+} and the contributions of various adsorption mechanisms were analysed. The adsorption mechanisms of Pb^{2+} included chiefly physisorption (Q_{phy}), ion exchange (Q_{exc}), precipitation (Q_{pre}), electrostatic (Q_{ele}) and complexation (Q_{com}) interactions. Based on the equilibrium experiments, montmorillonite, goethite, ferrihydrite and kaolinite were selected after adsorption of Pb^{2+} for stepwise extraction to quantify the adsorption mechanisms. In detail, 0.4 g of a sample was added into a centrifuge tube with 80 mL Pb^{2+} solution. When the adsorption process was complete, the adsorbent was washed with deionized water and the supernatant was removed. Following this, the prepared 20 mL of various extraction reagents were mixed with the Pb-loaded sample and were shaken for 24 h for Pb-loaded samples in deionized water and $NaNO_3$ solution, for 2 h for samples in $MgCl_2$ and for 5 h for samples in NaOAc. During the extraction process, the extracting reagents involved included deionized water, $MgCl_2$ at pH 7, NaOAc at pH 5 and 0.01 M $NaNO_3$. Finally, the contribution rate of each mechanism was calculated according to the adsorption/extraction capacity, and the effectiveness of the extracting reagent was obtained, which could be calculated according to Equations 1 & 2:

$$Q_i = V(C_0 - C_e)/m \tag{1}$$

$$R = (Q_i/Q) \times 100\% \tag{2}$$

where C_0 and C_e (mg L^{-1}) correspond to the initial and equilibrium concentrations of Pb^{2+}, Q (mg g^{-1}) is the total amount of adsorption, Q_i (mg g^{-1}) is the adsorption capacity corresponding to each adsorption mechanism, R is the proportion of each adsorption mechanism, m (g) is the weight of dried adsorbent and V (L) is the Pb^{2+} solution content.

Adsorption kinetics model

Two models (pseudo-first order (Equation 3) and pseudo-second order (Equation 4)) were used to fit the kinetics experimental data:

$$\ln(Q_e - Q_t) = \ln Q_e - k_1 t \tag{3}$$

$$\frac{t}{Q_t} = \frac{1}{k_2 Q_e^2} + \frac{1}{Q_e} \tag{4}$$

where Q_e and Q_t (mg g^{-1}) correspond to the adsorption capacities at equilibrium and time t (min), respectively, k_1 and k_2 represent the rate constants.

https://doi.org/10.1180/clm.2022.41 Published online by Cambridge University Press

Adsorption isotherm model

The isotherm experimental data were fitted to two adsorption isotherm models (Freundlich (Equation 5) and Langmuir (Equation 6)), with the parameters presented in Table 1.

$$\frac{C_e}{Q_e} = \frac{1}{Q_m K_L} + \frac{C_e}{Q_m} \quad (5)$$

$$\log Q_e = \frac{1}{n}\log C_e + \log K_F \quad (6)$$

where C_e (mg L^{-1}) refers to the equilibrium concentration, Q_e and Q_m (mg g^{-1}) are the equilibrium and saturated adsorption capacities, respectively, K_L and K_F are the adsorption rate constants implying the degree of adsorption, respectively, and $1/n$ is the heterogeneous factor.

Results and discussion

XRD characterization

The XRD traces of kaolinite, montmorillonite, goethite and ferrihydrite are shown in Fig. 1. These patterns matched well with the standard XRD traces of the four minerals. Information in the XRD traces allows identification of kaolinite, montmorillonite, goethite and ferrihydrite. No new reflections appeared after adsorption of Pb^{2+} by kaolinite, montmorillonite, goethite and ferrihydrite (Fig. 1), indicating that no new phase formed after the adsorption of Pb^{2+}. However, Fig. 1b showed that the peak intensity of montmorillonite after adsorption was weakened and the layer spacing was decreased. Layer spacing is one of the important factors reflecting the structural characteristics of montmorillonite, which can be calculated using the Bragg equation (Yu *et al.*, 2007). Specifically, the reflection that appeared at 5.86°2θ was consistent with the (001) plane of montmorillonite, and the corresponding layer spacing was 1.51 nm. The characteristic reflection located at 5.86°2θ was shifted to 6.17°2θ after the adsorption of Pb^{2+}. The layer spacing on the d_{001} surface of montmorillonite reduced from 1.51 to 1.43 nm after the adsorption of Pb^{2+}, illustrating that Pb^{2+} adsorption led to variation in the montmorillonite layer spacing, which was also demonstrated in Qu *et al.* (2018).

Table 1. Adsorption isotherm parameters of Pb^{2+} onto kaolinite, montmorillonite, goethite and ferrihydrite at pH 4–6.

		Langmuir			Freundlich		
Mineral	pH	Q_m	K_L	R^2	K_F	$1/n$	R^2
Kaolinite	4	10.1937	0.0137	0.7953	0.1973	0.7735	0.9562
	5	15.2905	0.0412	0.9730	1.0794	0.5708	0.9279
	6	18.6220	0.1297	0.9747	2.8576	0.4676	0.9204
Montmorillonite	4	66.1376	0.1575	0.9786	13.1066	0.3882	0.9896
	5	67.6133	0.4350	0.9887	25.6555	0.2370	0.9307
	6	69.2042	0.4544	0.9933	18.4103	0.3902	0.7735
Goethite	4	27.3598	0.0781	0.9323	5.6381	0.3282	0.9603
	5	31.2695	0.3402	0.9907	14.7737	0.1572	0.5166
	6	46.9484	0.5897	0.9958	14.9310	0.3140	0.6355
Ferrihydrite	4	21.5424	0.0196	0.9557	0.7140	0.6802	0.9878
	5	23.2558	0.0586	0.9952	2.3734	0.5041	0.9869
	6	34.3171	0.2435	0.9940	7.6057	0.3894	0.8336

SEM analysis

Kaolinite and montmorillonite both displayed a sheet-like morphology, while goethite and ferrihydrite showed a rod-like and irregular block-like morphology, respectively (Fig. 2a–h). The elemental composition of the four minerals was characterized using an energy-dispersive spectrometer (EDS) and elemental mapping. The results showed that the kaolinite presented a homogeneous distribution of Al, O and Si elements before adsorption (Fig. 2a,b). It was observed that O, Si, Al, Mg and Ca occurred in montmorillonite (Fig. 2c,d). Goethite and ferrihydrite were composed chiefly of Fe and O elements (Fig. 2e–h). No Pb element was found in the four minerals before adsorption, while the Pb element with various mass percentages of 5.16, 4.12, 2.84 and 3.47% was detected after adsorption. The above results confirmed that Pb^{2+} was adsorbed on the mineral surface.

FTIR spectroscopy analysis

FTIR spectroscopy was used to investigate the interaction mechanisms among the four minerals (kaolinite, montmorillonite, goethite and ferrihydrite) and Pb^{2+} related to various functional groups. O–H, Si–O, Al–O and other functional groups exist in the four minerals, among which O–H plays an important role in the adsorption process. In the case of kaolinite, internal and surface stretching of –OH corresponded to the peaks between 3620 and 3695 cm^{-1} (Fig. 3a; Mouni *et al.*, 2018). The intensities of all peaks caused by the –OH stretching modes were reduced due to the adsorption of Pb^{2+}. For montmorillonite, the bands at 1635 and 3412 cm^{-1} demonstrated the existence of the bending and stretching vibrations of adsorbed water (Fig. 3b). Both bands were reduced significantly after Pb^{2+} adsorption. The adsorption band at 3620 cm^{-1} represented structural –OH stretching (Liu *et al.*, 2013). The position of the structural –OH shifted to slightly greater wavenumbers after adsorbing Pb^{2+}, indicating that the –OH group participated in the adsorption process of Pb^{2+} (Wu *et al.*, 2011). Figure 3c shows that the adsorption peaks of goethite at 890 and 798 cm^{-1} were caused by the bending vibrations of Fe–OH, and the broad band at 3132 cm^{-1} illustrates the –OH stretching vibration of the group (Adebayo *et al.*, 2020). The results demonstrate that the peaks near 3132, 890 and 798 cm^{-1} broadened, revealing that –OH groups participated in the adsorption process. Ferrihydrite presented bands at 3354 and 1044 cm^{-1} related to the stretching vibration of structural –OH and the bending vibration of Fe–OH, respectively (Fig. 3d; Yang *et al.*, 2021). After the adsorption occurred, the peak located at 3354 cm^{-1} shifted to 3389 cm^{-1}, while the band at 1044 cm^{-1} demonstrated reduced intensity. These indicate the interaction of Pb^{2+} with the hydroxyl group on ferrihydrite (Gan *et al.*, 2019).

Adsorption kinetics

Figure 4 displays the relationship between contact time and the amounts of Pb^{2+} adsorbed by kaolinite, montmorillonite, goethite and ferrihydrite under batch experiments. The adsorption rates of the four minerals for Pb^{2+} were rapid, occurring within 5 min, and then gradually declined and became stable (Fig. 4). It has been speculated that the decreasing adsorptive sites occupied by Pb^{2+} reduce the adsorption rate (Zhang *et al.*, 2017; Penido *et al.*, 2019). Notably, Pb^{2+} adsorption on montmorillonite and goethite reached equilibrium within 20 min, while Pb^{2+} adsorption on kaolinite and ferrihydrite took 60 min to reach

https://doi.org/10.1180/clm.2022.41 Published online by Cambridge University Press

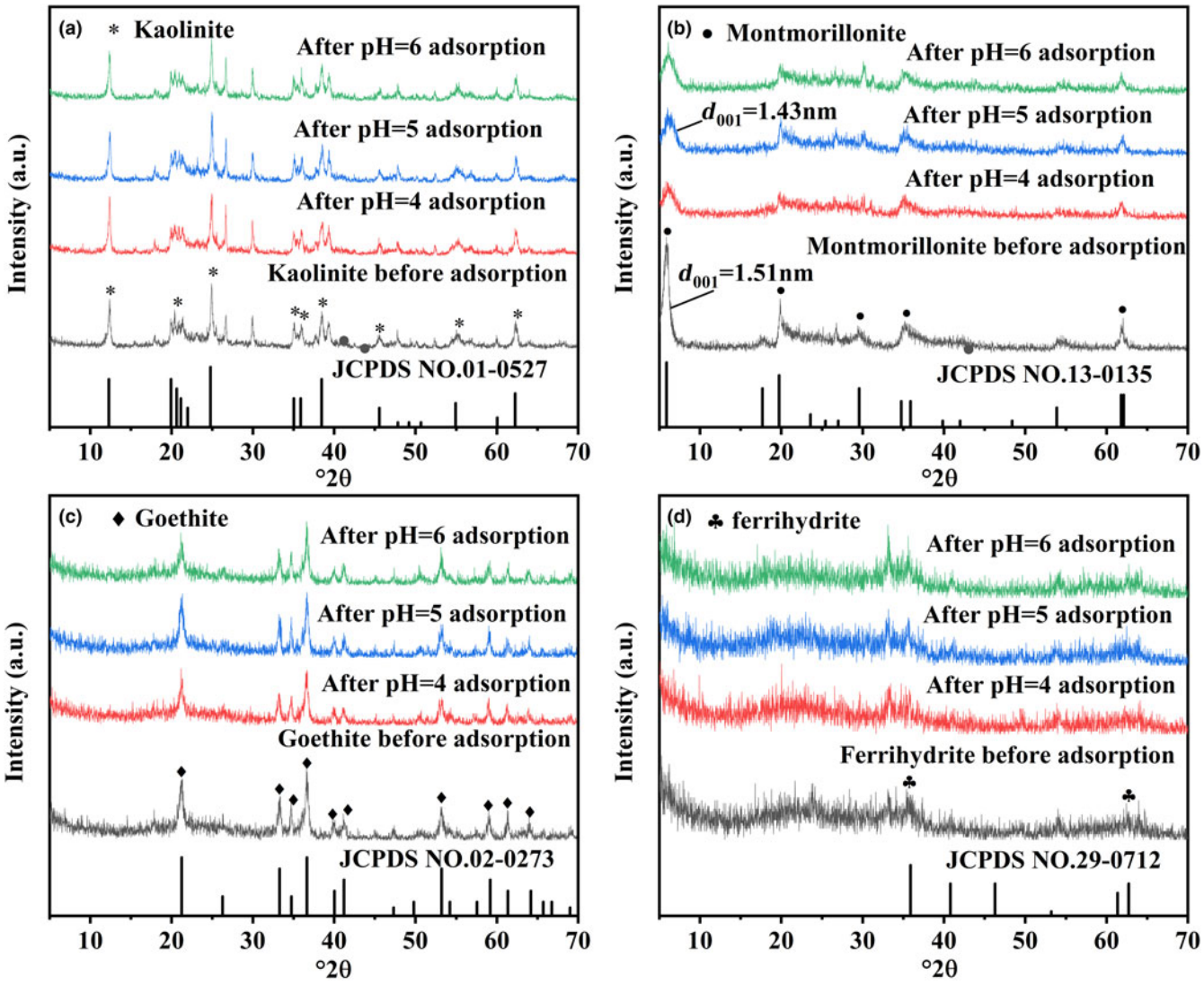

Fig. 1. XRD traces of (a) kaolinite, (b) montmorillonite, (c) goethite and (d) ferrihydrite before and after Pb^{2+} adsorption at pH 4–6.

equilibrium. The reason for this result might be the different mechanisms of adsorbing Pb^{2+} exhibited by the four minerals. The corresponding parameters are depicted in Table 2. The findings reveal that the adsorption process was more suitable for the pseudo-second order model ($R^2 > 0.98$), which indicates that Pb^{2+} adsorption on the four minerals was determined by chemisorption (Ahmad *et al.*, 2018; Jung *et al.*, 2019).

The pH value is a crucial factor in adsorption that can influence the surface charge of the adsorbent and the speciation of heavy metals in solution, which in turn affects the adsorption mechanism (Qu *et al.*, 2020a). Therefore, the surface properties of the four minerals were further tested using a ζ-potential analyser. The points of zero charge (pH_{pzc}) of kaolinite, goethite and ferrihydrite were determined to be ~2.84, 8.17 and 8.33, respectively, while montmorillonite was negatively charged at the tested pH values of 1–12 (Fig. 4i). It should be noted that lead presents primarily in the form of Pb^{2+} at the experimental pH values of 4–6 (Fig. 4j). Therefore, theoretically, montmorillonite and kaolinite demonstrated better Pb^{2+} adsorption performance than goethite and ferrihydrite, which might be due to electrostatic repulsion between goethite and ferrihydrite and the positive Pb^{2+} (Qu *et al.*, 2020a). However, the amount of Pb^{2+} adsorption of the various minerals was in the following order: montmorillonite > goethite > ferrihydrite > kaolinite (Fig. 4a–d). The excellent adsorption properties of montmorillonite might be caused by its high electronegativity and typical cation-exchange capacity (Zhu *et al.*, 2016). Nevertheless, the adsorption performance of kaolinite for Pb^{2+} was less impressive than that of goethite and ferrihydrite, although its pH_{pzc} was lower. This result reveals that electrostatic interaction was not the dominant mechanism determining the adsorption capacities of goethite, ferrihydrite and kaolinite. In addition, the adsorption capacities of the four minerals for Pb^{2+} demonstrated an upward trend with increasing solution pH, which could be attributed to the precipitation and complexation of Pb^{2+} on the four minerals at greater pH values. This was consistent with the stepwise extraction results showing that pH was correlated positively with precipitation and complexation.

Adsorption isotherms

The adsorption isotherms of Pb^{2+} on the four minerals are shown in Fig. 5. The adsorption capacities of the four minerals increased

https://doi.org/10.1180/clm.2022.41 Published online by Cambridge University Press

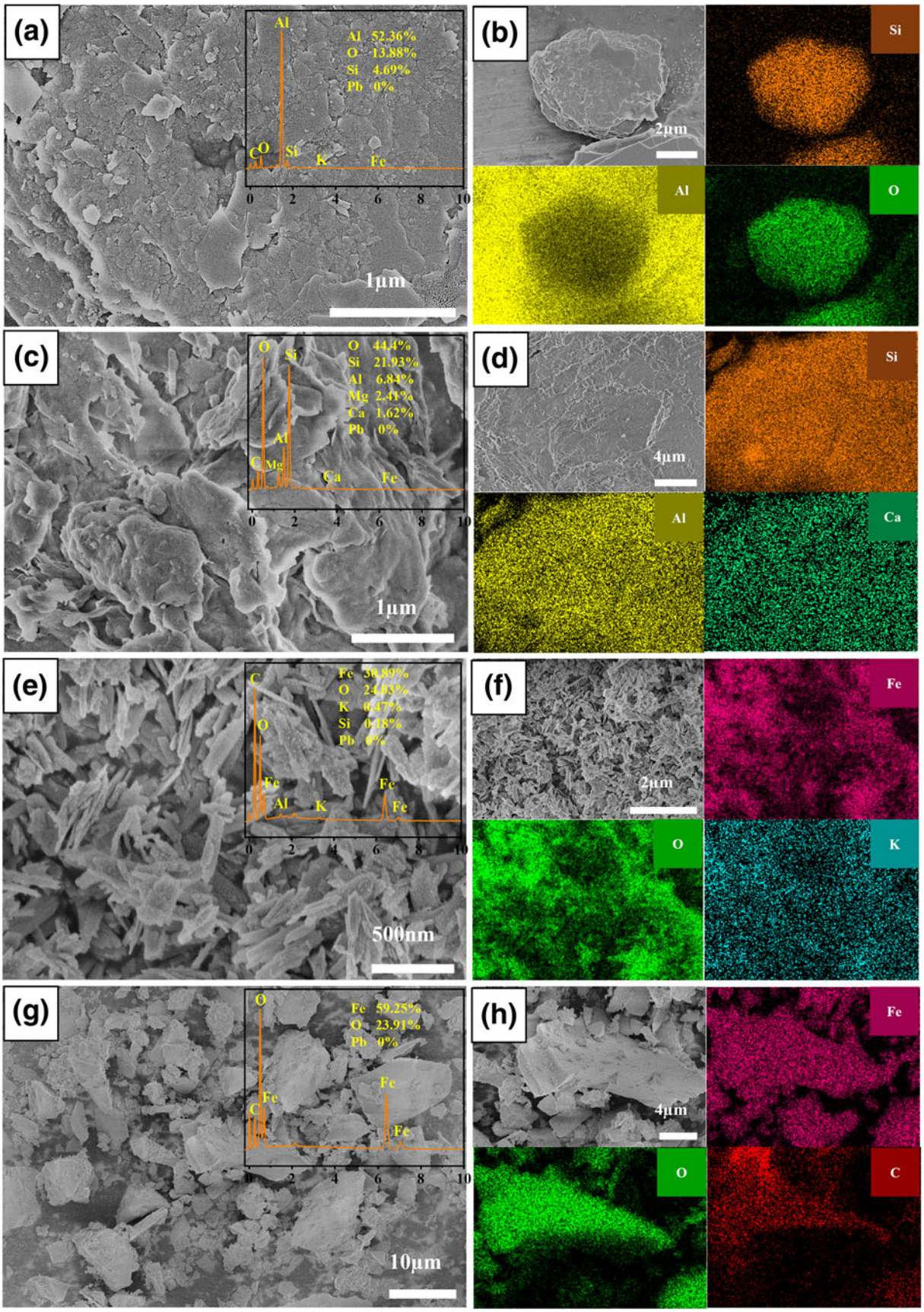

Fig. 2. SEM images, EDS spectra and elemental mapping images of the four minerals before and after Pb^{2+} adsorption. (a,b), (c,d), (e,f) and (g,h) represent kaolinite, montmorillonite, goethite and ferrihydrite before adsorption, respectively; (i,j), (k,l), (m,n) and (o,p) represent kaolinite, montmorillonite, goethite and ferrihydrite after adsorption at pH 6, respectively.

https://doi.org/10.1180/clm.2022.41 Published online by Cambridge University Press

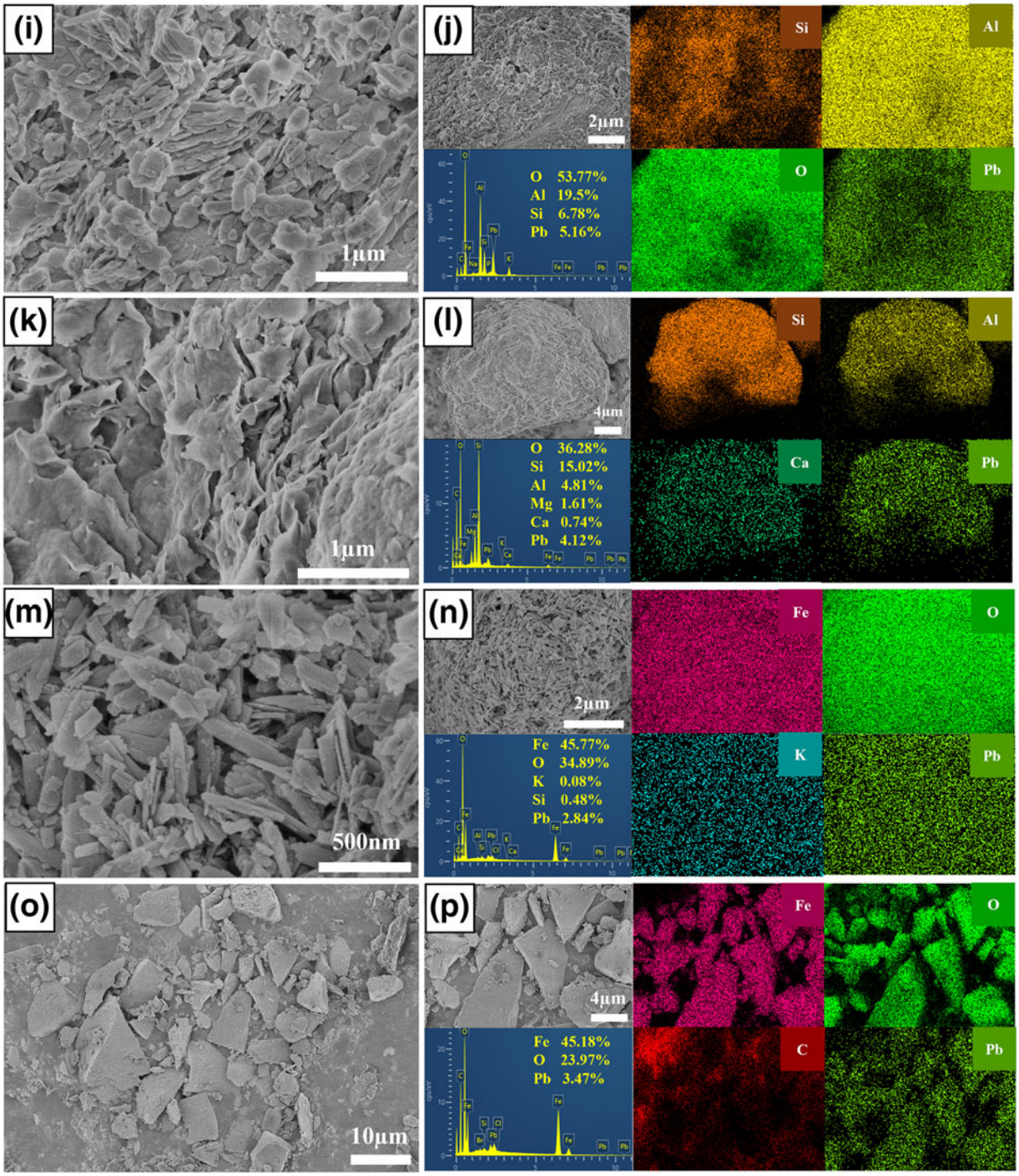

Fig. 2. (cont.)

rapidly with increasing Pb^{2+} concentration up to 50 mg L^{-1} and then increased more slowly to adsorption equilibrium. The adsorption properties of the four minerals for Pb^{2+} were compared. Note that montmorillonite showed the strongest adsorption performance for Pb^{2+} and kaolinite showed the weakest performance, which illustrates that Pb^{2+} adsorption on montmorillonite was outstanding. Moreover, the adsorption capacities of the four minerals were correlated positively with pH and increased with increasing pH, which was consistent with the kinetics results.

Langmuir and Freundlich models were used to simulate the obtained data, and the corresponding calculated parameters are listed in Table 1. The results demonstrate that the Freundlich isotherm better fit the Pb^{2+} adsorption data as shown by the greater R^2 value at pH 4, which indicates that the adsorption processes of the four minerals were mainly heterogeneous and represent multilayer adsorption. The Langmuir model ($0.97 < R^2 < 0.99$) of the four minerals showed a better fit effect than the Freundlich model ($0.51 < R^2 < 0.98$) at pH 5 and 6, illustrating that Pb^{2+} adsorption on the four minerals might be ascribed to the

https://doi.org/10.1180/clm.2022.41 Published online by Cambridge University Press

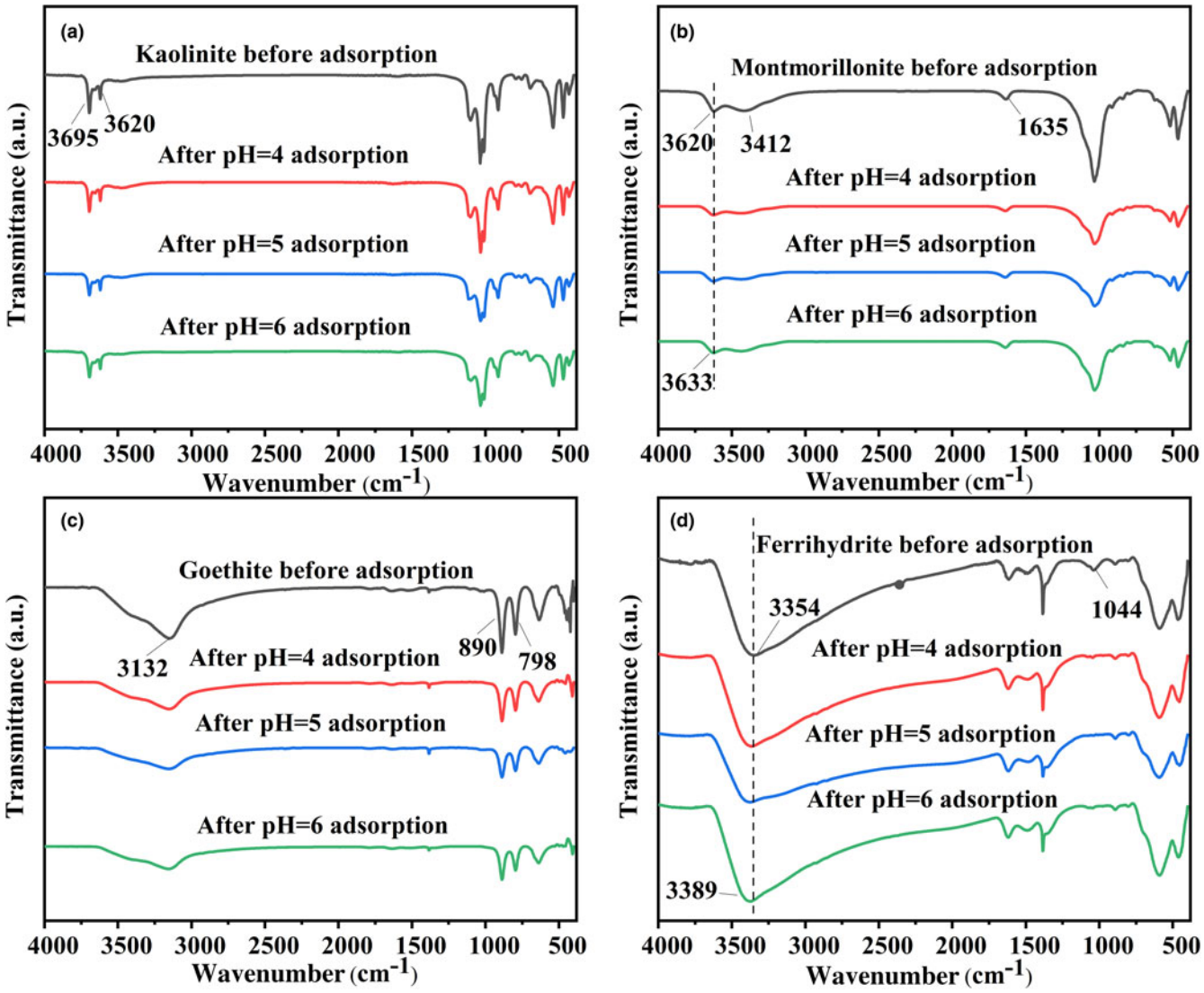

Fig. 3. FTIR spectra of (a) kaolinite, (b) montmorillonite, (c) goethite and (d) ferrihydrite before and after Pb^{2+} adsorption at pH 4, 5 and 6.

monolayer coverage of Pb^{2+} and homogeneous sites on the surface of the four minerals (Al-Ghouti & Da'Ana, 2020; Wu *et al.*, 2021). In addition, the total adsorption capacity of montmorillonite for Pb^{2+} was greater than that of kaolinite, goethite and ferrihydrite at pH 4–6. The maximum adsorption ability achieved for Pb^{2+} was 69.20 mg g^{-1} with montmorillonite at pH 6, whereas adsorption abilities reached 18.62, 46.95 and 34.32 mg g^{-1} with kaolinite, goethite and ferrihydrite, respectively, which was attributed to the typical cation-exchange capacity of montmorillonite. A relatively weak pH dependence was observed for montmorillonite adsorption, indicating that the main mechanism of montmorillonite adsorption was not pH-dependent complexation but the cation exchange between Pb^{2+} and the interlayer cations of montmorillonite (Chen & Kocar, 2018).

Adsorption mechanism of Pb^{2+}

The interactions that exist between soil minerals and metal ions are caused by multiple mechanisms (Gu *et al.*, 2019). To explore the Pb^{2+} adsorption mechanisms of the four minerals, the amount and contribution of each adsorption mechanism were quantified using a stepwise extraction method, and the results are depicted in Fig. 6. The contributions of physisorption for kaolinite, montmorillonite, goethite and ferrihydrite were 21.94–24.53, 1.02–1.87, 1.39–2.88 and 20.55–21.78% at pH 4–6, respectively. These results indicate that chemical action rather than physical action dominated the adsorption of Pb^{2+} by the four minerals. Regarding the adsorption process of Pb^{2+}, the four minerals demonstrated various adsorption mechanisms. For montmorillonite, the contribution of ion-exchange mechanism (R_{exc}) values ranged from 49.24 to 66.73% and decreased with increasing pH, indicating that ion exchange was the principal mechanism. Kaolinite, goethite and ferrihydrite all had smaller R_{exc} values than 18.91% and their contribution of complexation (R_{com}) values were greater than 38.38%, which imply that the adsorption mechanism of kaolinite, goethite and ferrihydrite was complexation rather than ion exchange. The adsorption mechanism determines the occurrence state of Pb^{2+} in soil, which affects the stability of the adsorbed Pb^{2+} accordingly. The Pb^{2+} adsorbed on the four minerals *via* physical interaction and cation exchange is unstable and highly bioavailable. By contrast, Pb^{2+} adsorbed through precipitation represents the partially bioavailable fraction, and the Pb^{2+}

https://doi.org/10.1180/clm.2022.41 Published online by Cambridge University Press

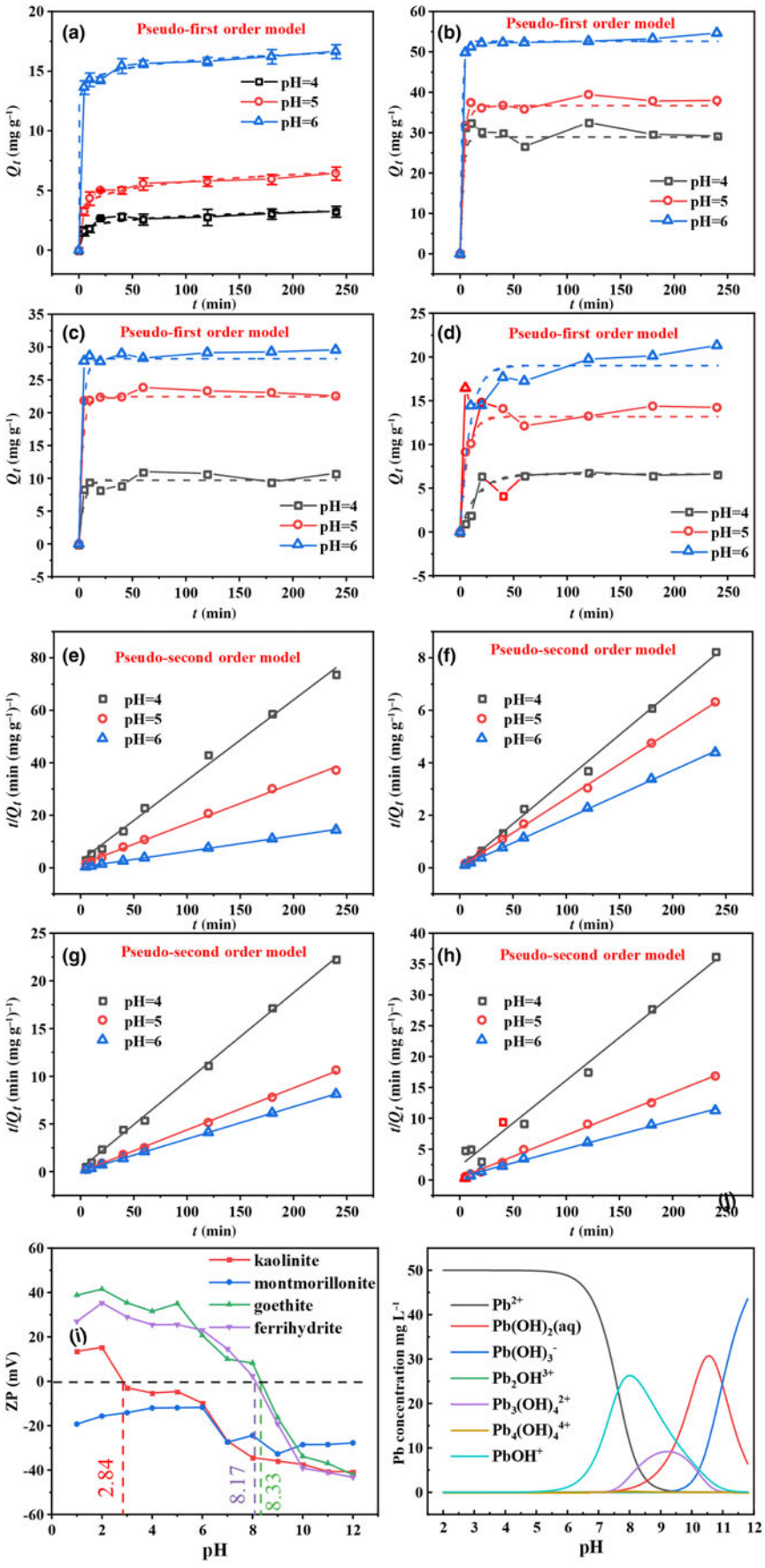

Fig. 4. (a–d) Pseudo-first order kinetics and (e–h) pseudo-second order kinetics of Pb^{2+} adsorption on kaolinite, montmorillonite, goethite and ferrihydrite at pH 4–6. (i) ζ-potentials (ZPs) of the four minerals under various pH conditions. (j) The species distributions of Pb^{2+} *vs* pH at the metal ionic concentration of 50 mg L^{-1}.

https://doi.org/10.1180/clm.2022.41 Published online by Cambridge University Press

Table 2. Adsorption kinetics parameters of Pb^{2+} onto kaolinite, montmorillonite, goethite and ferrihydrite at pH 4–6.

Mineral	pH	Pseudo-first order model			Pseudo-second order model		
		k_1	Q_e	R^2	k_2	Q_e	R^2
Kaolinite	4	0.0094	1.0921	0.6970	0.0418	3.2624	0.9945
	5	0.0093	2.1299	0.8420	0.0197	6.4400	0.9968
	6	0.0102	2.4936	0.9010	0.0189	16.6528	0.9995
Montmorillonite	4	−0.0064	1.0072	0.1930	−0.0530	29.5159	0.9968
	5	0.0043	3.8524	0.4925	0.0241	38.2555	0.9994
	6	0.0052	3.4876	0.7558	0.0123	54.3478	0.9996
Goethite	4	0.0100	2.3587	0.7900	0.0265	10.8472	0.9985
	5	0.0030	1.6265	0.3268	−0.0773	22.7583	0.9995
	6	0.0092	1.4507	0.7325	0.0305	29.5596	0.9999
Ferrihydrite	4	0.0114	2.9678	0.6286	0.0095	7.2031	0.9859
	5	0.0107	5.2849	0.9177	0.0123	14.4991	0.9976
	6	0.0096	6.1851	0.9003	0.0046	21.7770	0.9976

adsorbed through complexation is stable and harmless in soils. In brief, the great capacity of montmorillonite to adsorb Pb^{2+} was primarily due to the action of ion exchange, which only changes the occurrence state of Pb^{2+} and does not reduce environmental risk. The removal of Pb^{2+} *via* complexation with montmorillonite, kaolinite, goethite and ferrihydrite could reduce the readily bioavailable Pb^{2+}, thereby decreasing environmental risks.

The influence of pH on the Pb^{2+} adsorption of the four minerals was explored at an initial pH of 4–6. Figure 6a–d demonstrates that the adsorption capacity of montmorillonite was ~13.0, 1.5 and 2.5 times those of kaolinite, goethite and ferrihydrite, respectively, at pH 4–6, indicating the excellent adsorption performance of montmorillonite. The pH value of the solution affected considerably the contributions of various adsorption mechanisms, especially for montmorillonite (Pehlivan *et al.*, 2009). The pH value was correlated negatively with ion exchange and correlated positively with precipitation and complexation, which was attributed primarily to the increased pH and easier formation of metal hydroxides and carbonates (Fig. 6b; Zhong *et al.*, 2020). The contributions of electrostatic interactions to Pb^{2+} absorption on kaolinite and montmorillonite at pH 6 were 14.16 and 4.41%, respectively, while those for goethite and ferrihydrite were 0%. This was because kaolinite and montmorillonite were negatively charged at the experimental pH, while goethite and ferrihydrite were positively charged. Therefore, electrostatic interaction was involved in the uptake of Pb^{2+} by kaolinite and montmorillonite. Thus, pH value not only affected the adsorption mechanisms of the four minerals for Pb^{2+}, but also had an effect on the stability of the adsorbed Pb^{2+}. In general, considering the contributions of Pb^{2+} adsorption on the four minerals, it could be determined that pH value had the most critical effect on the Pb^{2+} adsorption process.

Conclusion

The Pb^{2+} adsorption capacities of kaolinite, montmorillonite, goethite and ferrihydrite were investigated. Furthermore, the contributions of various adsorption mechanisms at various pH values to remove Pb^{2+} were quantified using stepwise extraction experiments. The results illustrated that the four minerals had a significant capacity for Pb^{2+} removal. The kinetics of Pb^{2+} adsorption by the four minerals could be described well by the pseudo-second order model, indicating that the Pb^{2+} adsorption by the four minerals occurred mainly *via* chemical adsorption. Solution pH values affected the contributions of the various adsorption mechanisms considerably, especially for montmorillonite. Regardless of solution pH, the adsorption mechanisms of Pb^{2+} by montmorillonite and ferrihydrite were primarily ion exchange and complexation, accounting for 49.24–66.73 and 69.87–70.90%, respectively. The principal Pb^{2+} absorption mechanisms of kaolinite were

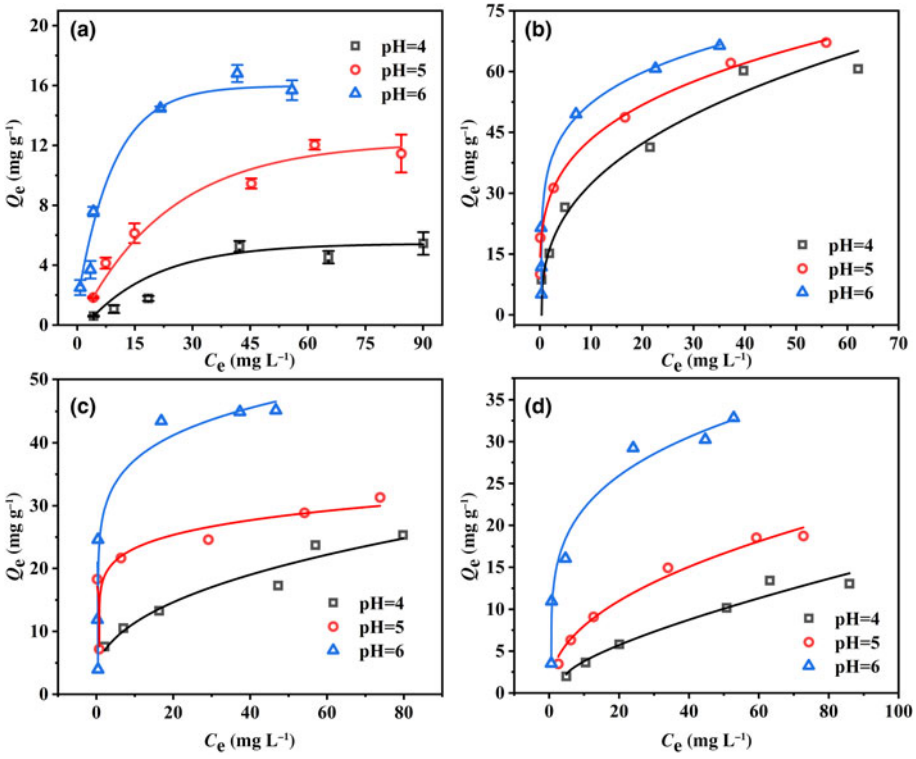

Fig. 5. Adsorption isotherms of Pb^{2+} on (a) kaolinite, (b) montmorillonite, (c) goethite and (d) ferrihydrite at pH 4–6.

https://doi.org/10.1180/clm.2022.41 Published online by Cambridge University Press

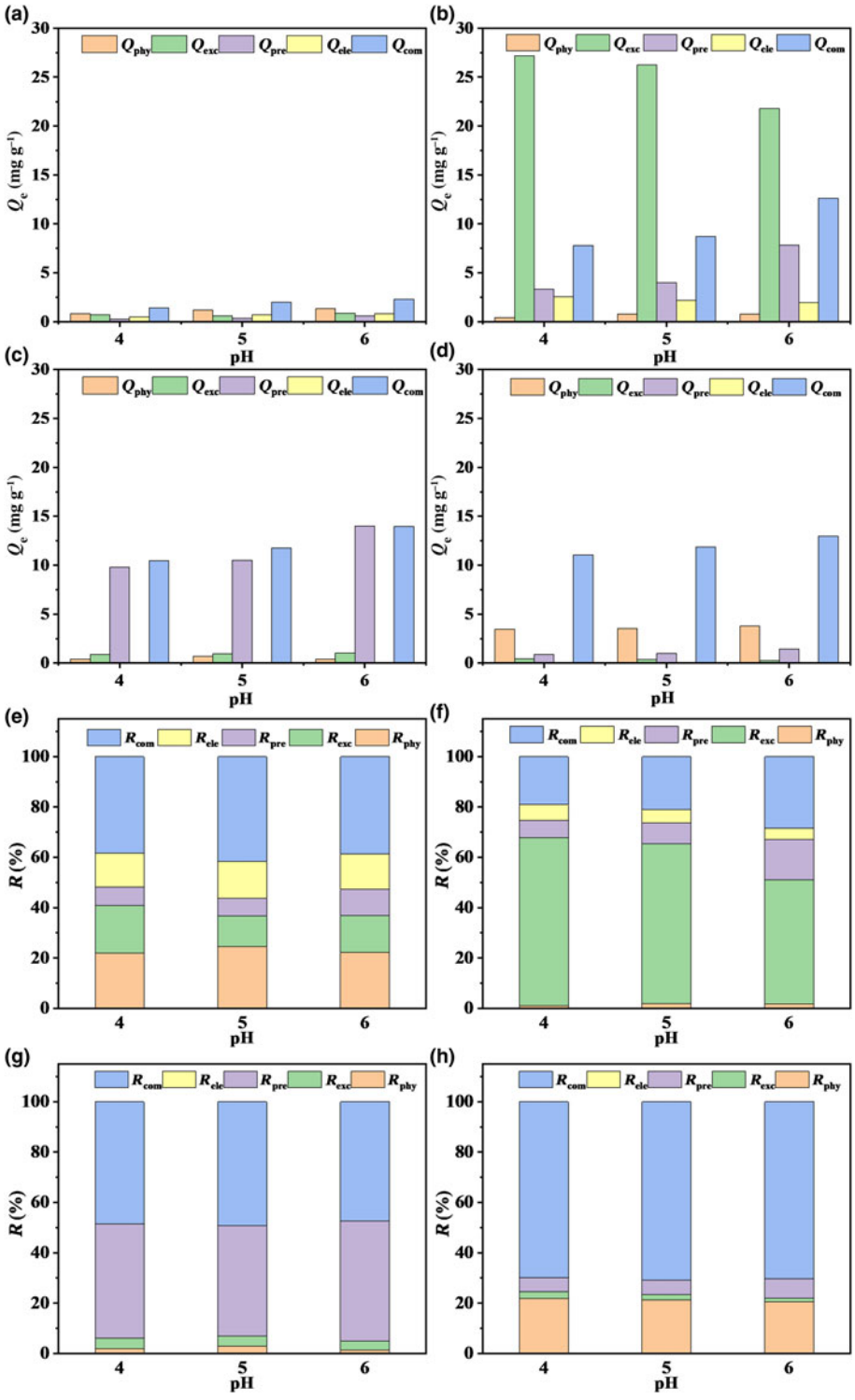

Fig. 6. Quantitative analysis of the (a–d) adsorption capacities and (e–h) contribution rates of the adsorption mechanisms of Pb^{2+} onto kaolinite, montmorillonite, goethite and ferrihydrite. Adsorption capacities are Q_{phy} for physisorption, Q_{exc} for ion exchange, Q_{pre} for precipitation, Q_{ele} for electrostatic and Q_{com} for complexation; contribution rates are R_{phy} for physisorption, R_{exc} for ion exchange, R_{pre} for precipitation, R_{ele} for electrostatic and R_{com} for complexation.

physical adsorption and complexation with a combined contribution of 60.32–66.23%, while those of goethite were precipitation and complexation with a combined contribution of 93.17–95.08%. These results, especially those from the stepwise experiments, improve our understanding of the fate of Pb^{2+} in soils.

Financial support. This research was supported by the Fundamental Research Funds for the Central Universities (PA2019GDQT0009).

Conflicts of interest. The authors declare none.

References

Adebayo G.B., Adegoke H.I. & Fauzeeyat S. (2020) Adsorption of Cr(VI) ions onto goethite, activated carbon and their composite: kinetic and thermodynamic studies. *Applied Water Science*, **10**, 213.

Ahmad Z., Gao B., Mosa A., Yu H., Yin X., Bashir A. *et al.* (2018) Removal of Cu(II), Cd(II) and Pb(II) ions from aqueous solutions by biochars derived from potassium-rich biomass. *Journal of Cleaner Production*, **180**, 437–449.

Al-Ghouti M.A. & Da'Ana D.A. (2020) Guidelines for the use and interpretation of adsorption isotherm models: a review. *Journal of Hazardous Materials*, **393**, 122383.

https://doi.org/10.1180/clm.2022.41 Published online by Cambridge University Press

Bedelean H., Măicăneanu A., Burcă S. & Stanca M. (2009) Removal of heavy metal ions from wastewaters using natural clays. *Clay Minerals*, **44**, 487–495.

Bourliva A., Michailidis K., Sikalidis C., Filippidis A. & Betsiou M. (2013) Lead removal from aqueous solutions by natural Greek bentonites. *Clay Minerals*, **48**, 771–787.

Cao Y., Xiao W., Shen G., Ji G., Zhang Y., Gao C. *et al.* (2019) Carbonization and ball milling on the enhancement of Pb(II) adsorption by wheat straw: competitive effects of ion exchange and precipitation. *Bioresource Technology*, **273**, 70–76.

Chen M.A. & Kocar B.D. (2018) Radium sorption to iron (hydr)oxides, pyrite, and montmorillonite: implications for mobility. *Environmental Science & Technology*, **52**, 4023–4030.

Fang Q., Chen B., Lin Y. & Guan Y. (2014) Aromatic and hydrophobic surfaces of wood-derived biochar enhance perchlorate adsorption *via* hydrogen bonding to oxygen-containing organic groups. *Environmental Science & Technology*, **48**, 279–288.

Gan W., Shang X., Li X., Zhang J. & Fu X. (2019) Achieving high adsorption capacity and ultrafast removal of methylene blue and Pb^{2+} by graphene-like TiO_2@C. *Colloids and Surfaces A: Physicochemical and Engineering Aspects*, **561**, 218–225.

Gu S., Kang X., Wang L., Lichtfouse E. & Wang C. (2019) Clay mineral adsorbents for heavy metal removal from wastewater: a review. *Environmental Chemistry Letters*, **17**, 629–654.

Guo Y.X., Liu J.H., Gates W.P. & Zhou C.H. (2020) Organo-modification of montmorillonite. *Clays and Clay Minerals*, **68**, 601–622.

Jung K., Lee S.Y., Choi J. & Lee Y.J. (2019) A facile one-pot hydrothermal synthesis of hydroxyapatite/biochar nanocomposites: adsorption behavior and mechanisms for the removal of copper(II) from aqueous media. *Chemical Engineering Journal*, **369**, 529–541.

Lai L., He Y., Zhou H., Huang B., Yao G. & Lai B. (2021) Critical review of natural iron-based minerals used as heterogeneous catalysts in peroxide activation processes: characteristics, applications and mechanisms. *Journal of Hazardous Materials*, **416**, 125809.

Lin J., Sun M., Su B., Owens G. & Chen Z. (2019) Immobilization of cadmium in polluted soils by phytogenic iron oxide nanoparticles. *Science of the Total Environment*, **659**, 491–498.

Liu D., Yuan P., Liu H., Cai J., Tan D., He H. *et al.* (2013) Quantitative characterization of the solid acidity of montmorillonite using combined FTIR and TPD based on the NH_3 adsorption system. *Applied Clay Science*, 80–81, 407–412.

Ma J., Lei M., Weng L., Li Y., Chen Y., Islam M.S. *et al.* (2019) Fractions and colloidal distribution of arsenic associated with iron oxide minerals in lead-zinc mine-contaminated soils: comparison of tailings and smelter pollution. *Chemosphere*, **227**, 614–623.

Mbaye A., Diop C.A.K., Miehe-Brendle J., Senocq F. & Maury F. (2014) Characterization of natural and chemically modified kaolinite from Mako (Senegal) to remove lead from aqueous solutions. *Clay Minerals*, **49**, 527–539.

Mouni L., Belkhiri L., Bollinger J., Bouzaza A., Assadi A., Tirri A. *et al.* (2018) Removal of Methylene Blue from aqueous solutions by adsorption on kaolin: kinetic and equilibrium studies. *Applied Clay Science*, **153**, 38–45.

Notini L., Latta D.E., Neumann A., Pearce C.I., Sassi M., N Diaye A.T. *et al.* (2018) The role of defects in Fe(II)-goethite electron transfer. *Environmental Science & Technology*, **52**, 2751–2759.

Otunola B.O. & Ololade O.O. (2020) A review on the application of clay minerals as heavy metal adsorbents for remediation purposes. *Environmental Technology & Innovation*, **18**, 100692.

Pehlivan E., Özkan A.M., Dinç S. & Parlayici S. (2009) Adsorption of Cu^{2+} and Pb^{2+} ion on dolomite powder. *Journal of Hazardous Materials*, **167**, 1044–1049.

Penido E.S., Melo L.C.A., Guilherme L.R.G. & Bianchi M.L. (2019) Cadmium binding mechanisms and adsorption capacity by novel phosphorus/magnesium-engineered biochars. *Science of the Total Environment*, **671**, 1134–1143.

Qu C., Du H., Ma M., Chen W., Cai P. & Huang Q. (2018) Pb sorption on montmorillonite–bacteria composites: a combination study by XAFS, ITC and SCM. *Chemosphere*, **200**, 427–436.

Qu J., Tian X., Jiang Z., Cao B., Akindolie M.S., Hu Q. *et al.* (2020a) Multi-component adsorption of Pb(II), Cd(II) and Ni(II) onto microwave-functionalized cellulose: kinetics, isotherms, thermodynamics, mechanisms and application for electroplating wastewater purification. *Journal of Hazardous Materials*, **387**, 121718.

Qu J., Yuan Y., Meng Q., Zhang G., Deng F., Wang L. *et al.* (2020b) Simultaneously enhanced removal and stepwise recovery of atrazine and Pb(II) from water using β-cyclodextrin functionalized cellulose: characterization, adsorptive performance and mechanism exploration. *Journal of Hazardous Materials*, **400**, 123142.

Ramola S., Belwal T., Li C.J., Wang Y.Y., Lu H.H., Yang S.M. *et al.* (2020) Improved lead removal from aqueous solution using novel porous bentonite–and calcite–biochar composite. *Science of the Total Environment*, **709**, 136171.

Rui D., Wu Z., Ji M., Liu J., Wang S. & Ito Y. (2019) Remediation of Cd- and Pb-contaminated clay soils through combined freeze–thaw and soil washing. *Journal of Hazardous Materials*, **369**, 87–95.

Schwertmann U. & Cornell R.M. (2008). *Iron Oxides in the Laboratory: Preparation and Characterization*. John Wiley & Sons, Hoboken, NJ, USA, 188 pp.

Shen Z., Zhang Y., Jin F., McMillan O. & Al-Tabbaa A. (2017) Qualitative and quantitative characterisation of adsorption mechanisms of lead on four biochars. *Science of the Total Environment*, **609**, 1401–1410.

Tang Q., Tang X., Li Z., Chen Y., Kou N. & Sun Z. (2009) Adsorption and desorption behaviour of Pb(II) on a natural kaolin: equilibrium, kinetic and thermodynamic studies. *Journal of Chemical Technology & Biotechnology*, **84**, 1371–1380.

Tessier A., Campbell P.G. & Bisson M. (1979) Sequential extraction procedure for the speciation of particulate trace metals. *Analytical Chemistry*, **51**, 844–851.

Trivedi P., Dyer J.A. & Sparks D.L. (2003) Lead sorption onto ferrihydrite. 1. A macroscopic and spectroscopic assessment. *Environmental Science & Technology*, **37**, 908–914.

Uddin M.K. (2017) A review on the adsorption of heavy metals by clay minerals, with special focus on the past decade. *Chemical Engineering Journal*, **308**, 438–462.

Vhahangwele M. & Mugera G.W. (2015) The potential of ball-milled South African bentonite clay for attenuation of heavy metals from acidic wastewaters: simultaneous sorption of Co^{2+}, Cu^{2+}, Ni^{2+}, Pb^{2+}, and Zn^{2+} ions. *Journal of Environmental Chemical Engineering*, **3**, 2416–2425.

Wu J., Wang T., Wang J., Zhang Y. & Pan W. (2021) A novel modified method for the efficient removal of Pb and Cd from wastewater by biochar: enhanced the ion exchange and precipitation capacity. *Science of the Total Environment*, **754**, 142150.

Wu P., Zhang Q., Dai Y., Zhu N., Dang Z., Li P. *et al.* (2011) Adsorption of Cu (II), Cd(II) and Cr(III) ions from aqueous solutions on humic acid modified Ca-montmorillonite. *Geoderma*, **164**, 215–219.

Yang K., Zhou C., Li C., Dou S., Li X., Wang X. *et al.* (2021) Efficient removal of Sb(V) in textile wastewater through novel amorphous Si-doped Fe oxide composites: phase composition, stability and adsorption mechanism. *Chemical Engineering Journal*, **407**, 127217.

Yin H., Tan N., Liu C., Wang J., Liang X., Qu M. *et al.* (2016) The associations of heavy metals with crystalline iron oxides in the polluted soils around the mining areas in Guangdong Province, China. *Chemosphere*, **161**, 181–189.

Yu J., Zeng X., Wu S., Wang L. & Liu G. (2007) Preparation and properties of montmorillonite modified asphalts. *Materials Science and Engineering: A*, **447**, 233–238.

Zhang J., Li L., Li Y. & Yang C. (2017) Microwave-assisted synthesis of hierarchical mesoporous nano-TiO_2/cellulose composites for rapid adsorption of Pb^{2+}. *Chemical Engineering Journal*, **313**, 1132–1141.

Zhang Y., Zou X., Liu H., Chen Y., Dong S., Ji M. *et al.* (2022) Comparative study of mineral with different structures supported Fe–Ni catalysts for steam reforming of toluene. *Fuel* (*Guildford*), **315**, 123253.

Zhong X., Chen Z., Li Y., Ding K., Liu W., Liu Y. *et al.* (2020) Factors influencing heavy metal availability and risk assessment of soils at typical metal mines in eastern China. *Journal of Hazardous Materials*, **400**, 123289.

Zhou S.Q., Niu Y.Q., Liu J.H., Chen X.X., Li C.S., Gates W.P. *et al.* (2022) Functional montmorillonite/polymer coatings. *Clays and Clay Minerals*, **70**, 209–232.

Zhu R., Chen Q., Zhou Q., Xi Y., Zhu J. & He H. (2016) Adsorbents based on montmorillonite for contaminant removal from water: a review. *Applied Clay Science*, **123**, 239–258.

https://doi.org/10.1180/clm.2022.41 Published online by Cambridge University Press